Diamond–metal contacts: interface barriers and real-time characterization

2009 J. Phys.: Condens. Matter 21 364223

(http://iopscience.iop.org/0953-8984/21/36/364223)

J. Phys.: Condens. Matter **21** (2009) 364223 (11pp) doi:10.1088/0953-8984/21/36/364223

Diamond–metal contacts: interface barriers and real-time characterization

D A Evans[1,3], O R Roberts[1], G T Williams[1], A R Vearey-Roberts[1], F Bain[1], S Evans[1], D P Langstaff[1] and D J Twitchen[2]

[1] Institute of Mathematics and Physics, Aberystwyth University, Aberystwyth SY23 3BZ, UK
[2] Element Six Ltd, Ascot, Berkshire SL5 8BP, UK

E-mail: a.evans@aber.ac.uk

Received 4 April 2009, in final form 7 June 2009
Published 19 August 2009
Online at stacks.iop.org/JPhysCM/21/364223

Abstract

A review of diamond–metal contacts is presented with reference to reported values of interfacial potential (Schottky) barriers and their dependence on macroscopic and microscopic properties of the diamond surface, the interface and the metal. No simple model can account for the overall spread of p-diamond barriers, although there are, for certain metals, correlations with metal electronegativity, interface chemistry and diamond surface preparation. Detailed studies are presented for a selected contact (Al—p-diamond) using real-time monitoring during metal growth from sub-nanometre to bulk films and subsequent *in situ* heating to 1000 °C. This contact, prepared in a clean vacuum environment on characterized single-crystal substrates, provides a case study for a combined *in situ* electrical and spectroscopic investigation using IV measurements for macroscopic diodes and real-time photoelectron spectroscopy for nanoscale metal films. Band bending during growth leads to a rectifying contact with a measured IV barrier height of 1.05 V and an ideality factor of 1.4. A transition from layered to clustered growth of the metal film is revealed in the real-time measurements and this is confirmed by AFM. For the annealed contact, a direct correlation is revealed by real-time photoemission between the onset of interfacial carbide formation and the change from a rectifying to an ohmic contact at 482 °C.

(Some figures in this article are in colour only in the electronic version)

1. Introduction

Diamond has many attributes that make it attractive as an alternative electronic and opto-electronic material to more conventional group IV, III–V and II–VI semiconductors. These include its mechanical, chemical and thermal stability [1], its retention of semiconducting properties at high temperature [2], its high thermal conductivity [3], its radiation hardness [4, 5], its bio-compatibility [6, 7], its large (UV) bandgap (5.5 eV) and its optical transparency. Examples of device applications and concepts based on diamond's unique properties include high temperature diodes [8], x-ray sensors [9] transfer-doped field effect transistors that use the negative electron affinity of H-terminated diamond surfaces [10, 11] and spin states for quantum computing [12]. Advances in CVD diamond growth have provided high-quality materials that are enabling many of these properties to be exploited in practical devices such as transistors and sensors [13]. The highest performance devices use high-quality single-crystal p-type CVD diamonds that are B-doped although n-type conductivity has been achieved and applied in devices using group V and group VI doping [14] and in nanocrystalline and ultrananocrystalline films [15, 16].

In device applications of semiconducting diamond, interfaces are often the ultimate limit to performance. Electron transport is, for example, affected by grain boundaries within the semiconductor, high contact resistance and energy alignment at heterointerfaces. In some cases (for example, high contact resistance), the interface properties are undesirable while in others (for example, diamond-adsorbate band alignment for transfer doping [17]) they are essential. While the effect of many of these interface properties can be included indirectly in device modelling, it is seldom possible to predict many of the important parameters and this is particularly true for the energy band alignment (energetics) at hybrid diamond

[3] Author to whom any correspondence should be addressed.

interfaces. In this paper, a review is presented of the current understanding of the metal–diamond interface (important for both rectifying Schottky contacts and low resistance ohmic contacts) and this is followed by a description of a new approach to probing the local chemical, physical and electronic structure for a selected metal–diamond contact using real-time monitoring at the nanoscale.

1.1. Metal–diamond interfaces

The degree of rectification of a metal–semiconductor diode is rarely predictable and diamond is no exception [18, 19]. The key parameter is the Schottky barrier height that is determined by the energetics at the metal–semiconductor interface and these are determined by intrinsic parameters such as the semiconductor electron affinity and the distribution of interface states at the metal–semiconductor junction [20]. In the simplest case of an ideal junction where the density of interface states is negligible, the barrier height for a given semiconductor is determined by the metal work function. At the other extreme of a large density of surface/interface states, the barrier height is independent of the metal work function and the energy imbalance is sustained by charge in the depletion region and in the interface states. In most cases, neither simple model can fully describe metal contacts to a given semiconductor, although an intermediate case of a weakly pinned Fermi level can be characterized by a parameter (the S parameter) that represents a linear variation between the two extremes. Coarsely, the S parameter increases with increasing bandgap for most common semiconductors, but diamond was identified at an early stage to be more likely to have a lower than expected value [21], with more recent measurements suggesting values of 0.7 [18] and 0.6 [19]. Where the S parameter is not unity, there arises a need to identify the nature of the pinning levels which, for diamond, lie low in the gap. Possible states include the diamond surface states, defect states or metal-induced states. The diamond surface states lie within the occupied and unoccupied bands [22] although their modification by adsorbates could provide the required states in the lower part of the bandgap. Defect states are commonly used to account for barriers on other semiconductors [20] although most of the common defect levels in diamond occur higher in the bandgap [1]. Metal-induced states that are derived from the diamond electronic states are predicted to result in pinning near an intrinsic energy (the charge neutrality level) and this level is predicted to lie deep in the bandgap for diamond [18, 23] While a weak work function dependence has been demonstrated for well-defined subsets of diodes [18, 23], there have been reported dependences of the diode rectification on surface morphology [24], surface termination [25, 26], interface oxides [27], interface chemistry [19, 25], temperature [19, 28, 29] and substrate doping [30]. This reflects the varied chemistry of metal–diamond interfaces [31] and the intrinsic properties of bulk diamond and diamond surfaces [22, 32].

1.2. Experimental measurement of barrier height

The Schottky barrier for p-type diamond is defined as the energy difference between the valence band maximum and the Fermi level at the metal–diamond interface. It is not always possible to directly determine this value for functional diodes, but it can be inferred in different ways using two main approaches. The first, for example using methods based on photoexcitation of electrons, is to measure the energy difference for a metal-free surface and then to measure changes in this value as very thin (<5 nm) metal films are grown on the surface. This approach requires a knowledge of the energetics of the starting surface. The second approach is to infer the barrier height from electrical or optical probes of diodes where the interface is buried under a thick metal contact in a device structure.

The most commonly applied techniques in these two approaches are photoelectron spectroscopy (PES) (using UV and x-ray sources) [33] and current–voltage (IV)/capacitance–voltage (CV) measurements [18], respectively. These are very different methods and do not necessarily yield the same values for a given system, although the spectroscopy has been shown in many cases to provide the explanation for the observed electrical measurements [34, 35]. Photoelectron spectroscopy is an established technique that provides a wealth of parallel information (e.g. interface bonding, density of occupied states, charge transfer, Fermi level shift). The main disadvantages of the technique are the need for an ultra-high-vacuum (UHV) environment, long data acquisition times and a finite probing depth. In conventional mode, it is not sensitive, for example, to changes during the transition from thin (<5 nm) to thick films ($\sim\mu$m) and cannot monitor device processing at realistic timescales or at ambient pressures. Advances in instrumentation (e.g. brighter tuneable light sources, efficient detection [36–39]) have enabled the technique to be applied in new ways that address many of these limitations (e.g. small area, high energy, high pressure and real time).

Electrical methods are applied to the completed device to provide direct measurement of parameters such as the barrier height but they are indirect probes of the interface since they are sensitive to all parts of the device structure. For example, current–voltage (IV) measurements may not provide accurate values of interface properties if charge transport is determined by factors other than the diamond–metal interface (e.g. insulating layers, bulk conductivity and inadequate ohmic contacts). Such techniques can only yield the true interface potential barrier if the current transport can be correctly modelled to take into account all the possible current transport mechanisms [20]. Often, all these effects are included in a modified thermionic-field emission model through the use of an 'ideality factor' (n). Where this factor significantly exceeds unity, the model should be considered as yielding an effective barrier height rather than the true interface potential barrier. Measurements of the metal–diamond barrier height determined by these two methods are summarized in figure 1.

The data are gathered from photoelectron spectroscopy [40, 33, 41–44, 24, 25, 45, 46] and IV/CV measurements [18, 47–49, 19, 50–53]; these are indicated by small and large points, respectively. The p-type barrier heights are plotted in relation to the diamond conduction band minimum and the valence band maximum. Also shown are the bulk p-type Fermi level position at 0.32 eV and the charge neutrality level

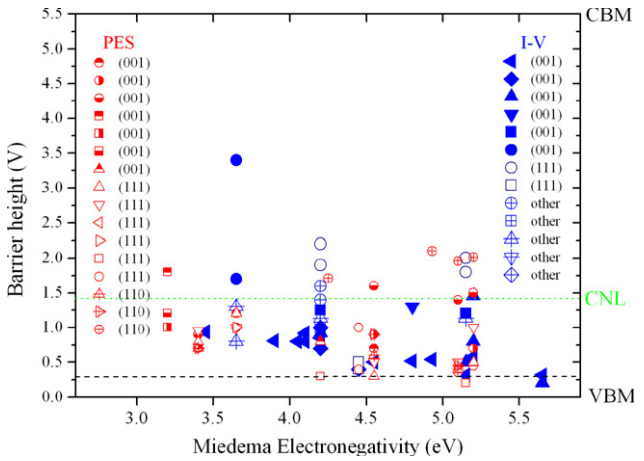

Figure 1. Schottky barrier heights for metal contacts on diamond. Data obtained by IV measurements are shown as the 3(001) surface. The most studied contacts are Al (at 4.2 eV) and Au (at 5.2 eV).

(CNL) at 1.4 eV [23]. The Fermi level positions for unmetallized surfaces lie at a range of values between these two positions. The metals are arranged in increasing electronegativity (the parameter chosen is that defined by Miedema [54] as it has been shown to be a more reliable parameter than either the work function or Pauling electronegativity for other semiconductors [23, 55]). The data points are further separated by crystal face: shaded or semi-shaded symbols represent (001), open symbols represent (111) and crossed symbols represent (110) for photoelectron spectroscopy measurements and unspecified or polycrystalline surfaces for IV/CV measurements.

In spite of the considerable scatter, it can be seen that, in general, there is a tendency towards lower barrier heights for higher electronegativity metals and this has been interpreted as a weak metal dependence corresponding to a small S parameter [23, 18, 19]. There is also a significant effect of surface processing, with oxygen-terminated surfaces generally yielding the highest barrier heights. Even where measurements have been reported on similar metal/surface combinations, there is often a wide scatter. This reflects the variation in material quality (some of the data are obtained for diamond epilayers grown on different substrates), differences in surface preparation methods and differences in data interpretation. In spite of this, it is evident that almost all values are clustered in the lower third of the bandgap (at or below the CNL) and there is a broad agreement between the values measured by *in situ* spectroscopy and electrical measurements. The first n-type materials are beginning to yield barrier height data and it seems that the high barriers measured [56] are consistent with pinning positions deep in the bandgap. While it is unlikely that any simple model can explain all the available data, with the improved availability of high-quality, reproducible single-crystal samples and better control of low resistance (ohmic) contacts, it is likely that subsets of interfaces will emerge where trends are evident, hence enabling predictability and control. There are currently very few reported p-type barrier heights outside the 0–1.5 V range [52], and so a more imaginative approach to band engineering is needed if large barriers on p-type diamond (or low barriers on n-type) are required. These could involve, for example, multi-layer fabrication and new functionalized surfaces. Such control measures require precise knowledge of the nanoscale properties of the interface and the first step is a knowledge of the chemical, electronic and structural properties of the diamond surface.

1.3. The diamond surface

The most widely used diamond surface in device applications is the O-terminated (001) surface prepared by O-plasma treatment or acid etching. Other common surfaces are the H-terminated surface that is obtained by H-plasma treatment and polishing with oil-based abrasives and the clean, reconstructed surface that is prepared in ultra-high vacuum by high temperature annealing. Although the (001) surface is the preferred substrate for CVD-grown material, similarly prepared surfaces of (111) termination are also widely studied since this is the natural cleavage plane for diamond and is also common in polycrystalline diamond films. There are also some studies on the (110) surface, although this is structurally less well defined. These surfaces have been the subject of many reviews dealing with surface orientation, termination, atomic and electronic structure [32, 18, 31].

The O-terminated (001) diamond surface has the same 2d periodicity as the ideal bulk-terminated crystal and the stabilization of the (1 × 1) surface has been proposed to be due to either atop (ketone) or bridging (ether) oxygen atoms although other terminations involving H and O species have been reported for water-exposed surfaces [57, 58] and O-exposed (110) surfaces [31]. This surface can be converted to the 2 × 1 O-free surface by high temperature removal of the oxygen atoms to form a reconstructed surface made up of sp^2-bonded carbon atoms. The H-terminated (001) surface has a 2 × 1 periodicity and this has been ascribed to H atoms adsorbed on the single dangling bond on each C atom in the reconstructed surface. This surface can be converted to the clean 2 × 1 surface by H desorption at high temperature [42, 59]. The (111) surface is somewhat different in that the unreconstructed, bulk-terminated surface is stabilized by H adatoms bonded to each sp^3 dangling bond. High temperature desorption results in a (2 × 1) surface made up of sp^2-bonded C atoms according to the Pandey model [60]. The O-terminated (111) surface, on the other hand, retains the (2 × 1) periodicity of the reconstructed surface.

The electronic states due to the surface atoms have been theoretically predicted and experimentally observed and these are mainly coincident in energy with the occupied (valence) and unoccupied (conduction) states of the bulk diamond rather than providing a high density of active states within the bandgap [32, 61]. However, the energy bands of each surface show various degrees of band bending near the surface that suggest that there are states within the bandgap of sufficient density to pin the Fermi level at a different position relative to the band edges compared to the bulk level. On p-diamond, all surface preparation methods result in gap states that, in general, pin the surface Fermi level deeper in the gap than the acceptor level, resulting in downward band bending at the surface. For example, the (111) surface Fermi level

for the C-terminated 2 × 1 surface lies further above the valence band maximum than that of the H-terminated 1 × 1 surface [42, 59]. There is a smaller difference between similarly prepared surfaces of different crystal orientation and there is some disagreement regarding the effect of oxygen termination, with some studies reporting the highest band bending for these surfaces [33] while others report the lowest band bending for the O-terminated (001) surface compared to the H-terminated and C-terminated surfaces [57]. The bulk Fermi level itself is less well defined in diamond than for other crystalline semiconductors. For example, highly B-doped diamond has a Fermi level position within the valence band and the material becomes metallic and, under certain conditions, superconducting [62].

In addition to causing a variation in surface Fermi level position relative to the band edges, the surface termination can have a more striking influence on its position relative to the vacuum level. The vacuum level for H-terminated surfaces lies below the conduction band, leading to a negative electron affinity. This effect leads to enhanced electron emission that has been exploited in cold-cathode emitters and has also been used to produce transfer-doped surface layers [63] in heterojunction-based intrinsic diamond transistors. These surface properties can be retained or enhanced in the presence of a metal overlayer [64] and the surface can have an influence for subsequent metal contact formation. In some cases, this is the dominant effect that offers a method for diode control based on surface modification. In other cases, chemical interaction dominates and there is a less clear influence of the starting substrate surface, notably for the carbide-forming ohmic junctions.

1.4. Diamond–metal chemistry

Diamond–metal chemistry can play an important role in determining electron transport and the interfaces can be grouped accordingly in general categories [18, 31]. At room temperature, diamond–metal interfaces are usually abrupt with little chemical disruption of the diamond surface. These form the first category of inert contacts and include metals such as Cu, Ag and Au. However, there is some evidence of bonding between Cu and diamond surfaces [65] and there is one suggestion that Au may diffuse into the diamond [66]. At higher temperatures, certain metals (e.g. Al, Ti, Mo, Ta, V) react with the diamond to form carbides [31, 67]: this is the second category. This chemical change is often accompanied by a change in the diode properties from Schottky to ohmic and this is perhaps the clearest correlation between device performance and chemistry. The preferred method for ohmic contact formation has evolved on this basis; Ti is the preferred contact metal as it forms a carbide at relatively moderate temperatures [68, 69]. The mechanism for this is not fully explained and it is interesting that the analogous silicide formation on silicon usually yields Schottky rather than ohmic contacts [20]. Other metals are often used along with Ti in ohmic contact formation as the barrier and contact layers [70]. Ohmic contacts have also been produced using other metal combinations [71], ion sputtering [72], increased surface doping [8] and graphitic contacts [19, 9]. The fourth category involves a small group of transition metals (notably Fe, Co and Ni) that induce graphitization of the diamond surface at temperatures as low as 450 °C [73]. Chemical effects are, however, sensitive to diamond surface orientation and functionalization as well as the processing environment and procedures and therefore detailed studies on individual interfaces are required to determine which of these have the strongest influence on the interfacial barrier.

1.5. The Al–diamond interface

To investigate further the correlation between temperature-induced bonding changes and contact resistance, a combined *in situ* electrical and photoelectron spectroscopy study has been carried out on Al contacts to single-crystal p-type diamond. In spite of its use as a rectifying contact in device applications [74], there is a large scatter in reported values for the Schottky barrier height. Values of between 0.8 and 2.2 V have been reported using a range of methods for variously prepared contacts [47, 48, 40, 75, 25, 50, 27] and these are shown in figure 1 for an electronegativity value of 4.2 eV. Although it is known that heating of these contacts can provide low resistance ohmic contacts, the transition temperature remains unclear. This is an important consideration for high temperature application of diamond electronics. For example, some studies report stable rectification at temperatures up to 430 °C [28, 76] while others have observed ohmic behaviour at such temperatures [77]. While there is agreement that Al contacts (in elemental or alloy form) can be used to fabricate ohmic contacts if annealed, there is less agreement on the temperature required to achieve this [75, 77, 31]. There is clearly no universal agreement on either the Al–diamond barrier height or the mechanism for ohmic contact formation and so a combined photoelectron spectroscopy and I–V approach has been applied to this junction, grown and measured under controlled conditions on a single-crystal surface to test the correlation between the techniques and also to minimize the influence of atmospheric oxidants. The combined electrical and spectroscopy system enables this transition to be monitored to probe correlations between electronic states, chemical bonding and device characteristics.

2. Experimental details

All *in situ* measurements were carried out in a UHV spectrometer equipped with sample heating, metal evaporation, fast photoelectron spectroscopy, low energy electron diffraction, metal contact masking and IV measurement. IV measurements were also carried out *ex situ* for diodes fabricated and measured in UHV. The UHV environment ensures a high degree of control of surface composition and structure and minimizes the effects of atmospheric contaminants. A B-doped ($N_B = 2 \times 10^{16}$ cm^{-3}) diamond (001) single crystal (Element Six Ltd) of dimensions 7.5 mm × 7.5 mm × 1.5 mm was polished and acid-etched prior to mounting in the UHV spectrometer. The bulk quality of this diamond was confirmed by Raman spectroscopy where the spectrum consists of a single narrow line at 1332.8 cm^{-1}, with a width of 1.6 cm^{-1}.

The surface composition, morphology and structure were characterized by photoelectron spectroscopy, low energy electron diffraction and atomic force microscopy (AFM). X-ray photoelectron spectroscopy (XPS) measurements were carried out using a Mg Kα x-ray source coupled to a commercial hemispherical analyser (VG CLAM4) modified by incorporation of a direct electron counting array detector developed at Aberystwyth [36]. The current detector has 768 channels distributed over 19 mm of the analyser focal plane, each with independent on-chip discrimination and amplifying electronics [37]. UV photoelectron spectroscopy using He I/He II radiation could also be performed in the same analysis chamber. The efficient detection system enables conventional high energy resolution spectroscopy to be complemented by real-time measurement of spectral features such as the C 1s core level photoelectron emission peak in snapshot mode. Real-time photoelectron spectroscopy is a relatively recent development that usually relies on intense incident radiation (most studies to data have been carried out at synchrotron light sources) coupled to efficient detectors [37–39]. In XPS mode, sufficient quality spectra could be measured in 1 s, a timescale that enables the growth of metal films to be monitored in real time using growth rates of around 0.2 nm min^{-1}. The surface sensitivity of the photoelectron technique when probing shallow core levels enables coverages from sub-monolayer to bulk (>10 nm) to be probed.

Indirect heating of the sample using a graphite/BN heater coupled to a programmable temperature ramping and data collection system enabled processing changes to be monitored from 20 to 1200 °C. Temperatures were estimated from a thermocouple secured on the sample holder close to the diamond, with values calibrated using an IR pyrometer in a separate but linked UHV chamber. Low energy electron diffraction patterns were recorded in the same environment as the PES and the surface topography was determined *ex situ* using a Park XE-100 AFM operated in contact mode. Metal layers were deposited from a shuttered Knudsen cell charged with high purity Al positioned in the photoelectron spectrometer for real-time studies and positioned in a connected UHV chamber equipped with aperture masks (1 mm diameter) and electrical probes for *in situ* I–V measurement. Ohmic back contacts were prepared by *in situ* heating of large-area Al contacts on the rear of the crystal. I–V characteristics were measured using a programmable Keithley 236 source/measurement unit.

3. Results and discussion

3.1. The diamond (001) surface

The acid-treated (001) surface was characterized using conventional XPS as shown in figure 2. The spectrum is dominated by the C 1s core level emission peak (at 969 eV) and the only other detectable element is oxygen (at 720 eV). The oxygen component, although small, persists throughout several heating cycles to 1000 °C, and a 1 × 1 surface periodicity as revealed by LEED is preserved. The C 1s peak for the as-loaded diamond consists of a single peak while there are at least two oxygen components. Following the first heating cycle to 400 °C, the lower BE oxygen component is removed and the remaining single peak (FWHM = 2 eV) is unchanged in shape at each subsequent heating stage. The relative oxygen abundance as a function of temperature is shown in the upper left-hand inset of figure 2. Although this steadily decreases with temperature, the O coverage remains sufficient to stabilize the unreconstructed 1 × 1 surface. Above 1000 °C, the O is rapidly desorbed as the reconstruction temperature is reached. This O-stabilized (001) surface following *in vacuo* annealing is a reproducible surface yielding the same binding energy and C 1s lineshape in many repeated acid etches and this is the surface chosen for both Al contact formation and real-time spectroscopic studies of the evolution of the room temperature Al–diamond Schottky contact and its transition to the high temperature carbide–diamond ohmic contact.

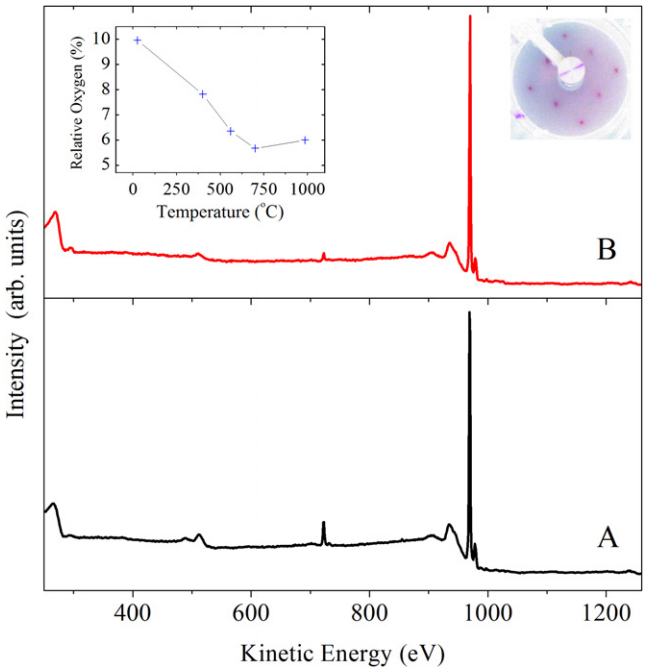

Figure 2. XPS spectra for the oxidized (001) diamond surface before (A) and after (B) *in vacuo* annealing to 800 °C. The relative attenuation of the O 1s peak at 720 eV is shown in the upper left inset. Following annealing, the surface shows a sharp 1 × 1 LEED pattern (upper right inset).

3.2. I–V measurements of Al–diamond contacts

A comparison of the IV characteristics for a heated Al contact and a room temperature grown contact is shown in figure 3. The left-hand panel shows data for two contacts that were fabricated *in vacuo* but measured *ex situ*. The unheated metal contact (solid line, curve A) is clearly rectifying, while the heated metal contact (dotted line, curve B) is almost symmetrical and indicates an ohmic contact with a resistance of around 20 kΩ. The forward characteristics of the unheated Al–diamond contacts (curve A) could be modelled using thermionic emission theory [20], with an ideality factor of 2. The right-hand panel shows data for rectifying diodes prepared

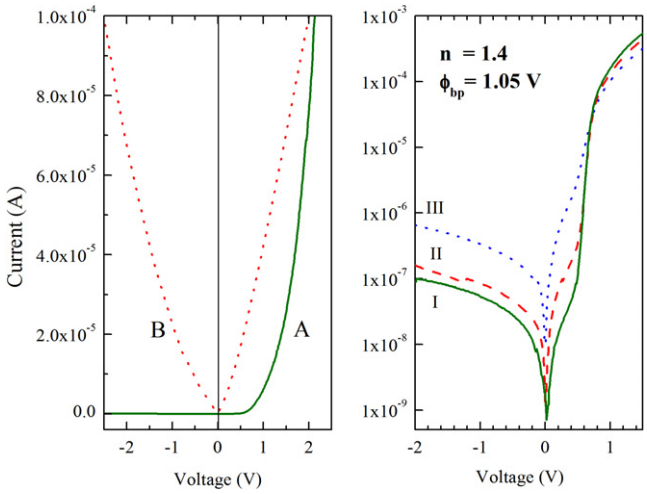

Figure 3. I–V characteristics for rectifying and ohmic contacts for Al on p-diamond (001). The left panel shows a rectifying Al–diamond contact (curve A) and a carbide–diamond ohmic contact (curve B) prepared by *in vacuo* annealing of an Al contact. The right panel shows IV characteristics for three Al–diamond diodes fabricated and sequentially measured (I–II–III) *in vacuo*. The ideality factor (n) and barrier height (ϕ_{bp}) are obtained by modelling the forward bias data of curve I.

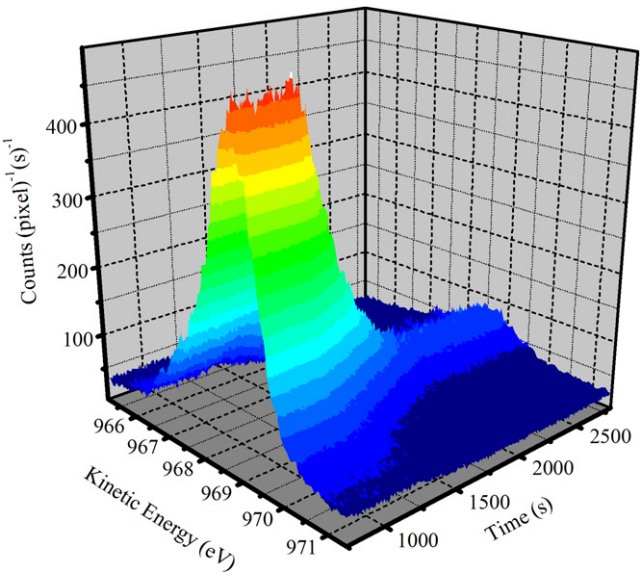

Figure 4. Real-time photoelectron spectroscopy of the growth of an Al contact on the diamond(001) surface. The C 1s core levels were recorded in 1 s snapshots.

and measured in UHV; these gave consistently higher-quality contacts with lower ideality factors. The quality degrades with time (curves I–III) and on removal from UHV. The most ideal diodes (curve I) yielded a barrier height of 1.05 V, with an ideality factor of around 1.4. This value of barrier height falls within the published range (figure 1) and is within 0.1 V of reported IV measurements with similar ideality factors [18, 31]. The linear (ideal diode) region of curve I extends over three orders of magnitude in current before the curve flattens above 0.7 V due to the effect of the series resistance. The deviation from linearity below 0.5 V is due to recombination–generation currents mediated by electronic states within the diamond bandgap [20]. The discrepancy in ideality factor between the *in situ* and *ex situ* measured diodes indicate a sensitivity to atmosphere that could account for the spread of reported values for barrier height evident in figure 1. A time-dependent degradation in diode quality was observed even for the diodes measured *in situ* (curves II and III were obtained by sequential measurement) indicating an increasing leakage resistance. The series resistance measured for all diodes was comparable to that of the ohmic contacts.

3.3. Real-time photoelectron spectroscopy of Al contact growth

Using an Mg Kα x-ray source, the growth of an Al film in UHV on the 1000 °C-heated 1 × 1 diamond(001) surface has been monitored by collecting sequential snapshot images of both the substrate C 1s peak and the overlayer Al 2s peak. A 6.3 eV energy window could be imaged across the 768-channel array for each core level at an analyser pass energy of 100 eV. The small pixel size ensured a sufficiently high energy resolution (FWHM ∼ 1 eV) and it was possible to record core level spectra in 1 s–10 s snapshots. The spectra were recorded sequentially during Al growth at a rate of 0.2 nm min^{-1} and data were collected for ∼1000 s before and after exposure of the diamond to the Al flux to confirm measurement stability. The total duration of each experiment was around 1 h. The time evolution of the C 1s core level is shown in figure 4. While there is a strong attenuation of the peak intensity during Al growth, there is little change in peak shape and it was possible to extract reliable intensity and peak position variation by fitting each snapshot with a single Gaussian/Lorentzian mix component. The intensity variation of the fitted C 1s core level peaks (figure 5) reveals the evolving morphology of the Al. Prior to exposure to the Al source, the peak intensity is stable, but it is rapidly attenuated beyond this point (shown as the first dotted vertical line in figure 5). At 2000 s, the Al flux ceases and no further attenuation is observed. On a semi-logarithmic plot (inset of figure 5), the data can be fitted by two straight lines. The initial attenuation is consistent with a layer-by-layer growth mode and the subsequent lower attenuation rate indicates cluster formation on the initial uniform film (i.e. a Stranski–Krastanov growth mode). The real-time experiment provides an accurate measurement of the critical thickness of the Al film of 1.51 nm that marks the transition from layered growth to clustered growth and also provides a value of 1.2 nm for the electron mean free path in the Al film.

The morphology of the Al film is confirmed by AFM measurements presented in figure 6. Images were recorded *ex situ* in contact mode under ambient conditions. The bottom image shows the edge of a 1 mm diameter Al contact similar to those used for I–V measurements. The height of the contact (18 nm) provides confirmation of the layer thickness estimated *in situ* by a quartz crystal oscillator placed in the Al flux. The upper left-hand image (A) taken on the unexposed diamond surface indicates the smoothness of the substrate. Few polishing lines are visible on a surface that has large flat

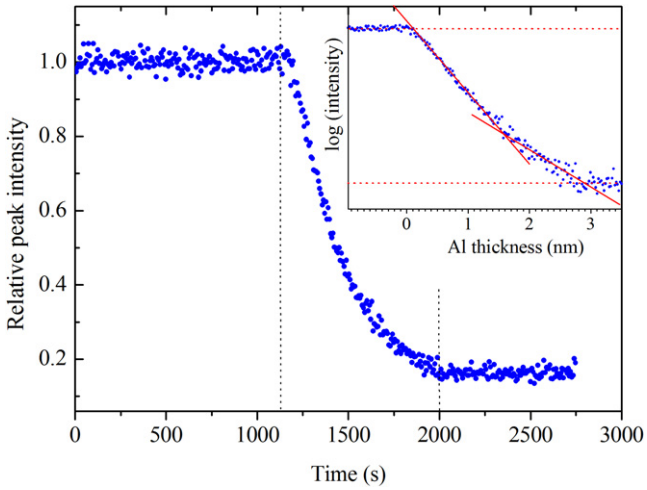

Figure 5. Variation of C 1s peak intensity as a function of time. The dotted lines represent the start and end points of the exposure of the diamond surface to the Al flux. The semi-logarithmic plot of intensity versus Al coverage in the inset gives a transition from layered to clustered growth at a thickness of 1.51 nm.

regions (0.2 nm roughness over 300 nm) with 1 nm undulations over larger distances. The surface of the Al film (upper right-hand image (B)) is significantly rougher, showing well-defined clusters of length 80 nm and height 1–1.5 nm. The film is, however, relatively uniform as predicted by the *in situ* spectroscopy measurements.

The energy position of the core level photoelectron emission peaks in a semiconductor is an indicator of the band edge position with respect to the Fermi level at the surface. Changes in peak position are therefore indicative of changes in band bending during processing of the material. The evolving energy shift observed in the diamond C 1s core level is shown in the left-hand panel of figure 7. The data shown are projections of the real-time spectra with colour representing peak intensity for both the C 1s core level of the diamond and the Al 2s core level of the growing metal film (right-hand panel). The C 1s peak shifts by a total of 260 meV to lower kinetic energy (higher binding energy) and the final position is attained at 2 nm Al coverage. This shift commences at very low Al coverages which are below the detection limit (figure 7) and there is little evidence of a corresponding shift in the Al 2s peak. This confirms the C 1s peak shift as due to a metal-induced change in band bending in the diamond. Such shifts have been observed in conventional photoelectron spectroscopy measurements for several metal–diamond interfaces [40, 33, 41–44, 24, 25, 45, 46] where a rectifying junction is formed. The total band bending can be calculated from this metal-induced value and the initial Fermi level position as determined from the substrate surface C 1s binding energy and the valence band edge measured using ultraviolet photoelectron spectroscopy (UPS). This band bending is comparable to the barrier height extracted from the IV data and so the photoelectron spectroscopy results are consistent with the electrical measurements for the room-temperature-grown Al contacts. A more detailed insight into

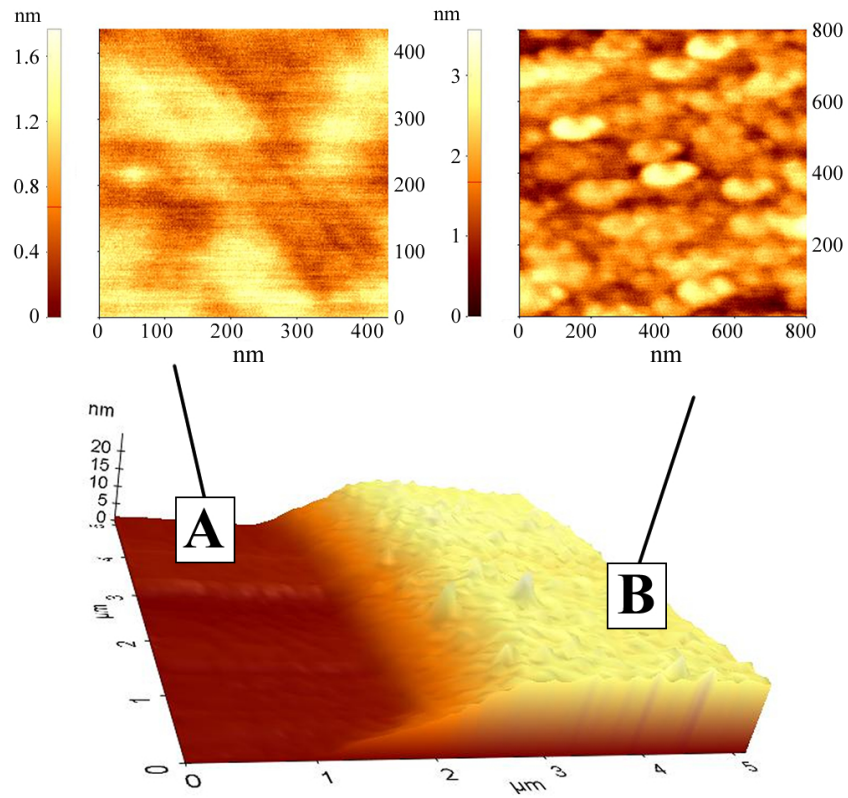

Figure 6. AFM images of the edge of an Al contact on the diamond (001) surface. The images were recorded in contact mode under ambient conditions. Images A and B are selected areas on the unexposed diamond surface and on top of the metal contact, respectively.

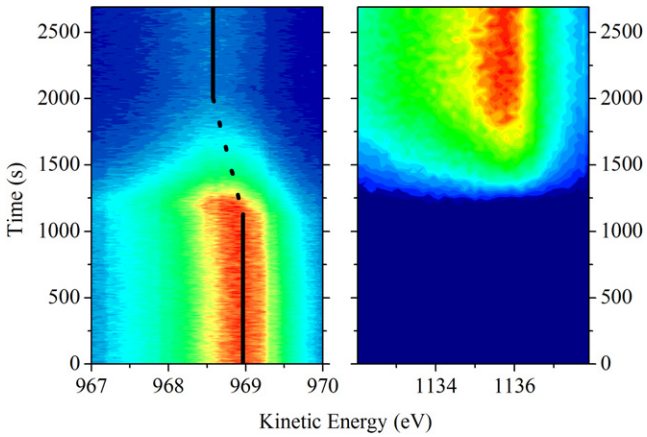

Figure 7. Projection views of the time (coverage) evolution of the diamond C 1s core level (left-hand panel) and the metal Al 2s core level (right-hand panel) during growth of an aluminium film on the diamond (001) surface. The line in the left hand panel is a guide to indicate the energy shift of the C 1s peak maximum.

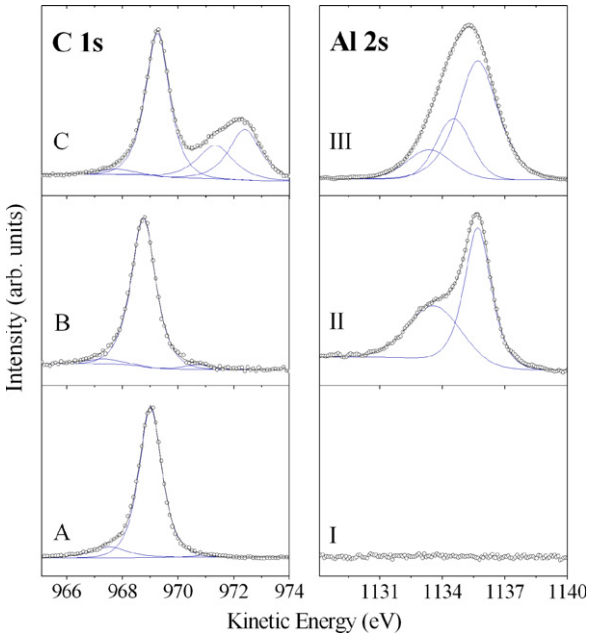

Figure 8. Fitted C 1s (left-hand panel) and Al 2s (right-hand panel) for the diamond (001) surface (curves A and I), the Al-exposed surface (curves B and II) and the annealed metallized surface (curves C and III). Open symbols represent the measured data points and solid lines represent the fit components and the total simulated curves.

the interface chemistry is obtained from curve fitting the C 1s and Al 1s for the clean, metallized and annealed surfaces as shown in figure 8.

All spectra are normalized to approximately equal height to allow comparison of the peak shape. The C 1s spectrum for the substrate diamond surface (curve A in figure 8) can be fitted using a dominant Gaussian/Lorentzian component at 969 eV, and two small components at lower (−1.5 eV) and higher (+1.9 eV) kinetic energy corresponding to surface carbon atoms. The fitted curves and their components are shown as the solid lines superimposed on the measured data points. The dominant diamond component has a consistent width of 0.92–0.99 eV for the acid-etched and annealed surface and this value is typical for clean diamond surfaces [31]. The relative intensity of the lower energy carbon peak (∼7%) is similar to the C:O ratio for these surfaces shown in figure 1 while the higher energy peak is considerably lower (∼1%). The former is identified as due to surface atoms bound to oxygen and the latter is due to surface sp^2-bonded carbon [31]. There is no structure in the region corresponding to the Al 2s core level emission for the initial diamond surface (curve I). Following adsorption of a 3 nm Al film, the C 1s core level peak (curve B) is unchanged in lineshape and can be fitted with the same two components, although there is a small reduction in the relative intensity of the C–O component and a corresponding increase in the relative intensity of the higher energy C component. The total intensity of these peaks relative to the main diamond peak remains unchanged. There is thus little apparent chemical interaction between the diamond and the Al at room temperature, in agreement with previous PES studies for Al on polycrystalline diamond [77]. All three C 1s components are shifted by 260 meV to lower kinetic energy and this rigid shift confirms the metal-induced change in band bending that results in a rectifying contact. On annealing to 860 °C, two new components appear in the C 1s emission spectrum at higher kinetic energy (curve C) indicating at least two new carbon-bonded species in the near-surface region. Additionally, the main diamond peak is shifted in energy by 0.52 eV to higher kinetic energy on annealing. This shift is opposite in sign to that observed on Al adsorption and is due to a reduction in the surface band bending at the diamond–Al interface that renders the contact less rectifying. The Al 2s core level emission spectra for the metallized surface (curve II in figure 8) consists of two components: the higher kinetic energy peak corresponds to elemental Al and a broader peak shifted by 2 eV to lower kinetic energy corresponds to Al–O bonding. The width of this oxide peak suggests that there is likely to be more than one oxide component, corresponding to different Al oxidation states. Its intensity is greater than that expected for Al adsorption onto the oxide-terminated diamond surface and the source of the additional oxide is most likely the residual gas within the spectrometer vacuum. The elemental Al peak is, however, dominant and the deposited film is metallic. On annealing *in vacuo*, the Al 2s emission spectrum changes shape significantly and cannot be fitted using the elemental and oxide components alone. The energy resolution is not sufficient to justify more than three components as shown in curve III in figure 8. The dominant peak appears close to the elemental Al energy but is broadened. The smallest peak is close to the binding energy of the oxide but has a reduced relative intensity and there is a third component at an intermediate energy. The binding energies of the carbide-related features in the C 1s and Al 2s emission spectra are similar to those reported for heated Al–polycrystalline contacts [77]. There are therefore at least three Al species in the annealed film involving bonding between the metal, carbon and oxygen. It is not possible to uniquely identify these phases or their spatial distribution within the contact from these spectra, but further

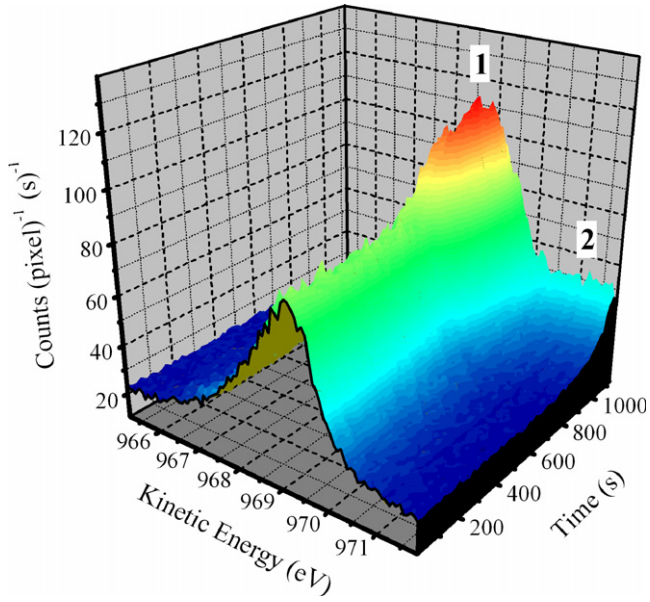

Figure 9. C 1s photoelectron emission spectra recorded in real time by integrating the electron signal detected at the analyser focal plane in a 6.3 eV window around 969 eV for 10 s per spectrum during the *in vacuo* annealing of a 3 nm Al film on diamond (001). The time axis represents a uniform heating ramp from room temperature to 860 °C. The main diamond peak (1) shifts and changes in intensity with temperature and additional electrons are emitted at higher kinetic energy (2).

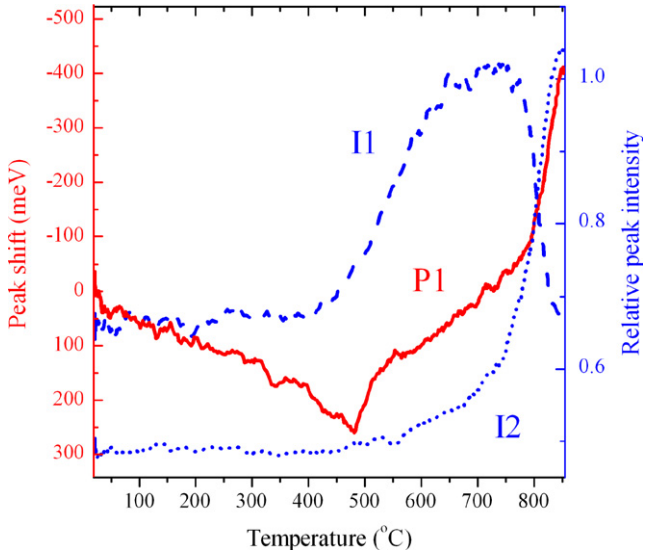

Figure 10. Temperature variation of the main spectral features of the C 1s core level for the metallized diamond (001) surface during *in vacuo* annealing. The solid line (curve P1) represents the peak position of the diamond peak component. The dashed line (curve I1) represents the intensity variation of this peak and the dotted line (curve I2) represents the intensity variation of the reacted carbide components.

insights into the evolving morphology and links between the changes in chemistry and interface energetics can be obtained from real-time monitoring of the annealing process [35]. The time dependence of the C 1s core level during annealing of an Al–diamond contact is shown in figure 9.

3.4. Real-time spectroscopy of in vacuo annealing

The temperature dependence of the Al–diamond interface was probed in real time by recording the C 1s core level in snapshot mode (10 s integration time per spectrum) during a programmed temperature ramping from room temperature to 860 °C at a rate of around 1.3 °C s^{-1} (figure 9). The main spectral changes are an increase in the peak intensity and the emergence of additional electron emission at higher kinetic energy (lower binding energy). There are also changes in the main diamond peak position as revealed in the top panel. The peak intensity reflects changes in morphology and chemistry and the peak position indicates changes in the relative Fermi level position at the surface. Since all these pieces of information are recorded in parallel, it is possible to probe their inter-relationships by following the time (temperature) evolution of the key spectral parameters of peak intensity and peak position as shown in figure 10.

The data presented in figure 10 were extracted by sequential fitting of the C 1s electron emission spectra shown in figure 9. The peak position of the diamond C 1s peak (P1), represented by the solid (red) line, initially shifts by around 250 meV to lower kinetic energy before abruptly changing direction at a temperature of 482 °C. This shift to higher kinetic energy continues as the temperature increases but the rate of shift increases sharply above around 800 °C. The initial shift is similar to that observed for the clean diamond surface and this unusual, reversible peak shift is believed to be due to a temperature-dependent Fermi level shift that increases the band bending at the surface. This is currently the subject of further study by real-time spectroscopy. The shift to higher kinetic energy at increased temperature is due to a reduction in the surface band bending and is hence an indication of a reduced potential barrier at the diamond–Al interface. The critical temperature of 482 °C thus indicates precisely the onset of the transition from a rectifying to an ohmic contact. Previous studies [28, 76, 77] have shown that Al–diamond contacts remain rectifying up to 430 °C in the absence of surface pre-sputtering [77]; this is just below the critical temperature measured here. The onset of ohmic behaviour nevertheless occurs at a lower temperature than previously believed for high-quality substrates and is lower even than the carbide onset temperature reported for Ti on diamond [69].

The corresponding peak intensity variation of the main diamond component of the C 1s emission spectrum is shown (I1) as the filled (blue) symbols in figure 10. There is little change in peak intensity up to a temperature of 410 °C, but the peak intensity increases by around 50% between 410 and 625 °C. This increase in substrate intensity is due to the onset of strong clustering of the Al film, exposing the substrate atoms. The clustering stabilizes during a further temperature increase of around 100 °C, before a sharp decrease in peak intensity commences at 750 °C. At this temperature, new chemical phases are formed on top of the substrate diamond, reducing the electron emission from these carbon atoms. This chemical reaction can be followed by monitoring

the integrated intensity of the additional carbide peaks that emerge at the high kinetic energy side of the diamond C 1s peak (figure 9). The time (temperature) variation of this peak (I2) is represented by the open (blue) symbols in figure 10. There is no electron emission above the background at these energies below around 480 °C. The intensity I2 increases slowly up to around 750 °C and then increases more rapidly at the highest temperatures. The formation of interface carbides therefore progresses in two regimes that are correlated with observed changes in both the peak intensity and position of the main diamond peak. The onset of reaction coincides with the sharp reversal point observed in the peak shift (P1) at 482 °C and this suggests a strong correlation between carbide formation and the transition from Schottky to ohmic for this contact. The onset of carbide formation is preceded by clustering of the Al film that commences around 410 °C and its low intensity suggests that this reaction is confined to the diamond surface atoms. A second transition point is identified at 750 °C where the rate of carbide formation increases sharply. This point of inflection in I2 is close to the point at which the intensity of the main diamond peak (I1) begins to decrease and so this represents the onset of Al reaction with the sub-surface diamond atoms to initiate bulk carbide formation. This rapid reaction is accompanied by an accelerated shift in the diamond C 1s peak position (P1) as the transition to an ohmic contact is completed.

4. Conclusion

The interface potential barrier heights for p-diamond–metal contacts have been reviewed and a weak metal dependence is revealed, indicating the influence of interfacial pinning states. All values are clustered in the lower part of the diamond bandgap close to the predicted charge neutrality level, but no single model can account for all the reported data points. For each metal, there is a spread in values that reflect the influence of processing and measurement and this has been discussed in terms of the substrate diamond surface and chemical interaction between the diamond and the metal. Both can have an influence on the barrier height. These observations are further illustrated by new measurements on the Al–diamond contact using *in situ* electrical measurements on macroscopic contacts and *in situ* real-time photoelectron spectroscopy on nanoscale films grown at room temperature and annealed to 860 °C. Electrical measurements yield an IV barrier height of 1.05 V with an ideality factor of 1.4 for Al grown in UHV on an O-terminated diamond(001) (1 × 1) surface. The quality of the diode characteristics deteriorates when removed from the UHV spectrometer and measured in air. Real-time spectroscopy studies of thin film growth reveal a transition from layered to weakly clustered growth of Al at a thickness of 1.51 nm. This morphology is confirmed by comparing AFM images of the unexposed diamond surface, the contact edge and the surface of the metal film. An increase in the diamond band bending is induced by metallization and the resultant potential barrier is consistent with the observed electrical measurements. Following high temperature annealing, IV measurements confirm the formation of a low resistance ohmic contact. The transition from rectifying to ohmic behaviour has been confirmed by real-time spectroscopy where a reversal in the observed surface Fermi level shift occurs at 482 °C. This temperature also marks the onset of an initial surface carbide formation that follows an enhanced clustering of the metal film at a slightly lower temperature of 410 °C. A sharp change in carbide reaction rate and diamond peak shift is initiated at a second transition temperature of 850 °C. The diamond peak intensity also decreases sharply at this point as the bulk reaction products bury the diamond surface. These measurements thus confirm a direct correlation between chemical reaction and contact conductivity and furthermore reveal that the carbide formation is a two-stage process involving first a surface reaction and then bulk reaction.

Acknowledgments

This work was supported by the EPSRC and Element Six Ltd and performed within the HEFCW Research and Enterprise Partnership at the Centre for Advanced Functional Materials and Devices (CAFMaD).

References

[1] Burns R C and Davies G J 1992 *The Properties of Natural and Synthetic Diamond* ed J E Field (London: Academic) pp 395–422
[2] Ye H, Tumilty N, Bevilacqua M, Curat S, Nesladek M, Bazin B, Bergonzo P and Jackman R B 2008 *J. Appl. Phys.* **103** 054503
[3] Baba K, Aikawa Y and Shohata N 1991 *J. Appl. Phys.* **69** 7313–5
[4] Pillon M, Angelone M, Aielli G, Almaviva S, Marinelli M, Milani E, Prestopino G, Tucciarone A, Verona C and Verona-Rinati G 2008 *J. Appl. Phys.* **104** 054513
[5] Tanaka T, Kaneko J, Takeuchi D, Sumiya H, Katagiri M, Nishitani T, Takeuchi H, Iida T and Ohkushi H 2001 *Rev. Sci. Instrum.* **72** 1406–10
[6] Tang L, Tsai C, Gerberich W W, Kruckeberg L and Kania D R 1995 *Biomaterials* **16** 483
[7] Hartl A, Schmich E, Garrido J A, Hernando J, Catharino S C R, Walter S, Feulner P, Kromka A, Steinmuller D and Stutzmann M 2004 *Nat. Mater.* **3** 736–42
[8] Twitchen D J, Whitehead A J, Coe S E, Isberg J, Hammersberg J, Wikstrom T and Johansson E 2004 *IEEE Trans. Electron Devices* **51** 826–8
[9] Sellin P J and Galbiati A 2005 *Appl. Phys. Lett.* **87** 093502
[10] Gi R S, Mizumasa T, Akiba Y, Hirose Y, Kurosu T and Iida M 1995 *Japan. J. Appl. Phys.* 1 **34** 5550–5
[11] Maier F, Riedel M, Mantel B, Ristein J and Ley L 2000 *Phys. Rev. Lett.* **85** 3472–5
[12] Dutt M V G, Childress L, Jiang L, Togan E, Maze J, Jelezko F, Zibrov A S, Hemmer P R and Lukin M D 2007 *Science* **316** 1312–6
[13] Isberg J, Hammersberg J, Johansson E, Wikstrom T, Twitchen D J, Whitehead A J, Coe S E and Scarsbrook G A 2002 *Science* **297** 1670–2
[14] Koizumi S, Watanabe K, Hasegawa F and Kanda H 2001 *Science* **292** 1899–901
[15] Kulkarni P, Porter L M, Koeck F A M, Tang Y J and Nemanich R J 2008 *J. Appl. Phys.* **103** 084905
[16] Gerbi J E, Auciello O, Birrell J, Gruen D M, Alphenaar B W and Carlisle J A 2003 *Appl. Phys. Lett.* **83** 2001–3

[17] Ristein J 2006 *Science* **313** 1057–8
[18] Kawarada H 1996 *Surf. Sci. Rep.* **26** 205–59
[19] Chen Y G, Ogura M and Okushi H 2004 *J. Vac. Sci. Technol.* B **22** 2084–6
[20] Rhoderick E H and Williams R H 1988 *Metal–Semiconductor Contacts* (Oxford: Clarendon)
[21] Ihm J, Louie S G and Cohen M L 1978 *Phys. Rev. Lett.* **40** 1208–11
[22] Sque S J, Jones R and Briddon P R 2006 *Phys. Rev.* B **73** 085313
[23] Monch W 1996 *J. Vac. Sci. Technol.* B **14** 2985–93
[24] Tachibana T, Williams B E and Glass J T 1992 *Phys. Rev.* B **45** 11975–81
[25] Maier F, Riedel M, Ristein J and Ley L 2001 *Diamond Relat. Mater.* **10** 506–10
[26] Saby C and Muret P 2002 *Diamond Relat. Mater.* **11** 851–5
[27] Kiyota H, Matsushima E, Sato K, Okushi H, Ando T, Kamo M, Sato Y and Lida M 1995 *Appl. Phys. Lett.* **67** 3596–8
[28] Hewett C A and Zeidler J R 1993 *Diamond Relat. Mater.* **2** 1319–21
[29] Rodrigues A M 2008 *J. Appl. Phys.* **103** 083708
[30] Shiomi H, Nishibayashi Y and Fujimori N 1991 *Japan. J. Appl. Phys.* 1 **30** 1363–6
[31] Evans S 1992 *The Properties of Natural and Synthetic Diamond* ed J E Field (London: Academic) pp 181–214
[32] Ristein J 2006 *Appl. Phys.* A **82** 377–84
[33] Baumann P K and Nemanich R J 1998 *J. Appl. Phys.* **83** 2072–82
[34] Vearey-Roberts A R and Evans D A 2005 *Appl. Phys. Lett.* **86** 072105
[35] Evans D A, Roberts O R, Vearey-Roberts A R, Langstaff D P, Twitchen D J and Schwitters M 2007 *Appl. Phys. Lett.* **91** 132114
[36] Langstaff D P, Bushell A, Chase T and Evans D A 2005 *Nucl. Instrum. Methods* B **238** 219–23
[37] Langstaff D P and Chase T 2007 *Nucl. Instrum. Methods* A **573** 169–71
[38] Gregoratti L, Barinov A, Benfatto E, Cautero G, Fava C, Lacovig P, Lonza D, Kiskinova M, Tommasini R, Mahl S and Heichler W 2004 *Rev. Sci. Instrum.* **75** 64–8
[39] Nambu A, Bussat J-M, West M, Sell B C, Watanabe M, Kay A W, Mannella N, Ludewigt B A, Press M, Turko B, Meddeler G, Zizka G, Spieler H, van der Lippe H, Denes P, Ohta T, Hussain Z and Fadley C S 2004 *J. Electron Spectrosc. Relat. Phenom.* **137–140** 691–7
[40] Himpsel F J, Heimann P and Eastman D E 1980 *Solid State Commun.* **36** 631–3
[41] Baumann P K, Bozeman S P, Ward B L and Nemanich R J 1997 *Diamond Relat. Mater.* **6** 398–402
[42] Vanderweide J and Nemanich R J 1994 *Phys. Rev.* B **49** 13629–37
[43] Baumann P K and Nemanich R J 1998 *Phys. Rev.* B **58** 1643–54
[44] Vanderweide J and Nemanich R J 1992 *J. Vac. Sci. Technol.* B **10** 1940–3
[45] Muret P, Pruvost F, Saby C, Lucazeau E, Tan T A N, Gheeraert E and Deneuville A 1999 *Diamond Relat. Mater.* **8** 961–5
[46] Muret P, Gheeraert E and Deneuville A 1999 *Phys. Status Solidi* a **174** 129–35
[47] Mead C A and McGill T C 1976 *Phys. Lett.* A **58** 249–51
[48] Hicks M C, Wronski C R, Grot S A, Gildenblat G S, Badzian A R, Badzian T and Messier R 1989 *J. Appl. Phys.* **65** 2139–41
[49] Chen Y G, Ogura M and Okushi H 2003 *Appl. Phys. Lett.* **82** 4367–9
[50] Takeuchi D, Yamanaka S, Watanabe H, Okushi H and Kajimura K 2000 *Appl. Surf. Sci.* **159** 572–7
[51] Denisenko A, Aleksov A, Pribil A, Gluche P, Ebert W and Kohn E 2000 *Diamond Relat. Mater.* **9** 1138–42
[52] Craciun M, Saby C, Muret P and Deneuville A 2004 *Diamond Relat. Mater.* **13** 292–5
[53] Ri S G, Nebel C E, Takeuchi D, Rezek B, Tokuda N, Yamasaki S and Okushi H 2006 *Diamond Relat. Mater.* **15** 692–7
[54] Miedema A R, Dechatel P F and Deboer F R 1980 *Physica* B+C **100** 1–28
[55] Von der Emde M, Zahn D R T, Schultz C, Evans D A and Horn K 1992 *J. Appl. Phys.* **72** 4486–7
[56] Suzuki M, Yoshida H, Sakuma N, Ono T, Sakai T and Koizumi S 2004 *Appl. Phys. Lett.* **84** 2349–51
[57] Gao X Y, Liu L, Qi D C, Chen S, Wee A T S, Ti O Y, Loh K P, Yu X and Moser H O 2008 *J. Phys. Chem.* C **112** 2487–91
[58] Laikhtman A, Lafosse A, Le Coat Y, Azria R and Hoffman A 2004 *Surf. Sci.* **551** 99–105
[59] Cui J B, Ristein J and Ley L 1998 *Phys. Rev. Lett.* **81** 429–32
[60] Pandey K C 1982 *Phys. Rev.* B **25** 4338–41
[61] Palummo M, Pulci O, Del Sole R, Marini A, Schwitters M, Haines S R, Williams K H, Martin D S, Weightman P and Butler J E 2005 *Phys. Rev. Lett.* **94** 087404
[62] Yokoya T, Nakamura T, Matsushita T, Muro T, Takano Y, Nagao M, Takenouchi T, Kawarada H and Oguchi T 2005 *Nature* **438** 647–50
[63] Strobel P, Riedel M, Ristein J and Ley L 2004 *Nature* **430** 439–41
[64] Lubbe M, Evans D A, Kampen T U, Okano K and Zahn D R T 1999 *Diamond Relat. Mater.* **8** 1485–9
[65] Wang X G and Smith J R 2001 *Phys. Rev. Lett.* **8718** 186103
[66] Zhen C M, Wang Y Y, He S H, Guo Q F, Yan Z J and Pu Y J 2003 *Opt. Mater.* **23** 117–21
[67] Evans S and Ney M R 1990 *J. Hard Mater.* **1** 169–81
[68] Moazed K L 1992 *Metall. Trans.* A **23** 1999–2006
[69] Viljoen P E, Lambers E S and Holloway P H 1994 *J. Vac. Sci. Technol.* B **12** 2997–3005
[70] Werner M, Dorsch O, Baerwind H U, Obermeier E, Johnston C, Chalker P R and Romani S 1995 *IEEE Trans. Electron Devices* **42** 1344–51
[71] Looi H J, Pang L Y S, Whitfield M D, Foord J S and Jackman R B 2000 *Diamond Relat. Mater.* **9** 975–81
[72] Zhen C M, Wang Y Y, Guo Q F, Zhao M, He Z W and Guo Y P 2002 *Diamond Relat. Mater.* **11** 1709–12
[73] Clifton P H and Evans S 1995 *Indust. Diamond Rev.* **55** 26–31
[74] Mori Y, Kawarada H and Hiraki A 1991 *Appl. Phys. Lett.* **58** 940–1
[75] Chen Y G, Ogura A, Yamasaki S and Okushi H 2004 *Diamond Relat. Mater.* **13** 2121–4
[76] Chan S S M, Peucheret C, McKeag R D, Jackman R B, Johnston C and Chalker P R 1995 *J. Appl. Phys.* **78** 2877–9
[77] Tachibana T and Glass J T 1992 *J. Appl. Phys.* **72** 5912–8